JOURNAL OF Materials CHEMISTRY

Crystal structures and magnetic properties of the 6H-perovskites $Ba_3LnRu_2O_9$ (Ln = Ce, Pr and Tb)

Yoshihiro Doi,*[a] Makoto Wakeshima,[a] Yukio Hinatsu,[a] Aya Tobo,[b] Kenji Ohoyama[b] and Yasuo Yamaguchi[b]

[a]*Division of Chemistry, Graduate School of Science, Hokkaido University, Sapporo 060-0810, Japan*
[b]*Institute for Materials Research, Tohoku University, Sendai 980-8577, Japan*

Received 12th June 2001, Accepted 18th September 2001
First published as an Advance Article on the web 23rd October 2001

Magnetic properties of quaternary oxides $Ba_3LnRu_2O_9$ (Ln = Ce, Pr and Tb) are reported. These compounds adopt the 6H-perovskite structure with space group $P6_3/mmc$, in which the cation sites within the face-sharing octahedra are occupied by Ru ions and those within the corner-sharing octahedra are occupied by Ln ions. The oxidation states of both Ru and Ln ions were found to be tetravalent. These compounds are semiconductors over the temperature range 100–400 K. Measurements of the magnetic susceptibility and specific heat were carried out. The Ln^{4+} antiferromagnetic transition occurred at 9.5 K for Ln = Tb and 10.5 K for Ln = Pr. Powder neutron diffraction measurements for $Ba_3TbRu_2O_9$ were performed at 2 and 15 K, and at room temperature. It was found that $Ba_3TbRu_2O_9$ has a long range antiferromagnetic ordering of Tb^{4+} ions at 2 K. The moments of the Tb^{4+} ions order ferromagnetically in the c plane, and these ferromagnetic planes are stacked antiferromagnetically along the c axis. The direction of the ordered moments is parallel to the c axis, and the ordered magnetic moment of the Tb^{4+} ions is 6.84(4) μ_B.

Introduction

It is well known that perovskite and perovskite-like oxides containing ruthenium ions often exhibit interesting magnetic and electrical properties.[1,2] In such oxides, the perovskites containing both ruthenium and lanthanide ions are of particular interest for the study of magnetic cooperative phenomena due to interactions between d and f electrons. Recently, a series of ordered perovskites, A_2LnRuO_6 (A = Sr, Ba; Ln = Y, lanthanides), have been investigated, and various magnetic behaviors have been observed at low temperatures.[3–7]

We now turn our attention to the magnetic properties of the ruthenium-based oxides having a 6H-$BaTiO_3$-type structure,[8] which have the general formula $Ba_3MRu_2O_9$ (M = 3d transition metals, lanthanide elements, *etc.*). In many cases, these compounds have a hexagonal unit cell. The Ru and M ions occupy the face-sharing octahedral sites (Ru_2O_9 dimer) and the corner-sharing octahedral sites (MO_6 octahedron), respectively. Previously, Darriet *et al.* reported that the temperature dependence of the magnetic susceptibilities of $Ba_3M^{2+}Ru^{5+}{}_2O_9$ (M = Mg, Ca, Cd and Sr), which show broad maxima at 400–500 K.[9] This behavior is explained by the antiferromagnetic Ru^{5+}–Ru^{5+} coupling in the isolated Ru_2O_9 dimer.[9,10] If the M^{2+} ions are magnetic, another magnetic interaction should operate between the Ru^{5+} and M^{2+} ions, and long range magnetic ordering may be observed. In fact, $Ba_3NiRu_2O_9$ and $Ba_3CoRu_2O_9$ show antiferromagnetic transitions (T_N of the former is 95 K).[11,12]

If the M ions are lanthanides, magnetic cooperative phenomena due to the interaction between d and f electrons may be observed. Thumm *et al.* reported that $Ba_3LnRu_2O_9$ (Ln = Y, La, Nd, Sm–Gd, Dy–Yb) adopted a 6H-$BaTiO_3$-type structure.[13,14] Rath and Müller-Buschbaum measured the magnetic susceptibility of $Ba_3LnRu_2O_9$ (Ln = Y, Gd and Yb) above 77 K.[15] They showed that the Gd and Yb compounds obey the Curie–Weiss law, while the Y compound does not. Very recently, we have reported the magnetic properties of $Ba_3NdRu_2O_9$ using powder neutron diffractometry and some magnetic measurements.[16] It was found that this compound has a charge configuration of $Ba_3Nd^{3+}Ru^{4.5+}{}_2O_9$, and that it shows a structural phase transition at *ca.* 120 K and a ferromagnetic transition of Nd^{3+} ions at 24 K.

In this paper, we focus our attention on $Ba_3LnRu_2O_9$ (Ln = Ce, Pr and Tb). The most stable oxidation state of lanthanide ions is trivalent. In addition to this, cerium, praseodymium and terbium may also be found in the tetravalent state. The Ce and Pr compounds are known to adopt a charge configuration of $Ba_3Ln^{4+}Ru^{4+}{}_2O_9$.[14,17] $Ba_3TbRu_2O_9$ may also have the same charge configuration. It is expected that these three compounds will show many interesting magnetic properties due to the magnetic behavior of the $Ru^{4+}{}_2O_9$ dimer and the magnetic interactions between the Ru^{4+} and Ln^{4+} ions. In order to elucidate their magnetic properties, we have measured the magnetic susceptibility, specific heat, electrical resistivity and neutron diffraction patterns, which will be reported here.

Experimental

Polycrystalline samples of $Ba_3LnRu_2O_9$ (Ln = Ce, Pr and Tb) were prepared by a conventional solid-state reaction. $BaCO_3$, RuO_2, CeO_2, Pr_6O_{11} and Tb_4O_7 were used as starting materials. They were weighed out in the appropriate metal ratio and well mixed in an agate mortar. The mixtures were pressed into pellets and then calcined at 900 °C for 12 h. The calcined materials were initially fired in air at 1100 °C for 24 × 2 h, and were thereafter fired at 1200 °C for 24 × 4 h (Ln = Ce) or at 1200 °C for 24 × 2 h and at 1300 °C for 24 × 4 h (Ln = Pr, Tb) with several interval grindings and pelletings. The heating-up rate was 100 °C h^{-1}.

The powder X-ray diffraction profiles for all samples were measured in the range $10° \leqslant 2\theta \leqslant 120°$ using a 2θ step size of 0.02° with Cu-Kα radiation on a Rigaku MultiFlex diffractometer.

Powder neutron diffraction profiles for $Ba_3TbRu_2O_9$ were

DOI: 10.1039/b105134m

measured at 2 and 15 K, and at room temperature in the range $3^\circ \leqslant 2\theta \leqslant 153^\circ$ at intervals of 0.1° with a wavelength of 1.8196 Å. Measurements were performed on the Kinken powder diffractometer for high efficiency and high resolution measurements, HERMES, of the Institute for Materials Research (IMR), Tohoku University,[18] installed at the JRR-3M Reactor in the Japan Atomic Research Institute (JAERI), Tokai. Crystal and magnetic structures were determined by the Rietveld technique, using the program RIETAN2000.[19]

The magnetic measurements were carried out using a SQUID magnetometer (Quantum Design, MPMS-5S). The temperature dependence of the magnetic susceptibilities was measured under both zero-field-cooled (ZFC) and field-cooled (FC) conditions in an applied field of 0.1 T over the temperature range 1.8–400 K.

Specific heat measurements were performed using a relaxation technique with a heat capacity measurement system (Quantum Design, PPMS model) in the temperature range 1.8–300 K. The sintered sample in the form of a pellet was mounted on a thin alumina plate with grease for better thermal contact.

The temperature dependence of the resistivity was measured in the temperature range 100–400 K (for both cooling and heating processes) using a DC four-probe technique with the same measurement system (PPMS model). The sintered samples were cut into pieces of approximately $9.5 \times 3.0 \times 0.9$ mm^3. Four contacts were painted onto the samples using silver paste.

Results and discussions

Crystal structures

The results of the X-ray diffraction (XRD) measurements show that the $Ba_3LnRu_2O_9$ (Ln = Ce, Pr and Tb) compounds are formed as a single phase. The X-ray diffraction patterns of the Ce and Pr compounds are shown in Fig. 1. The data have been analyzed by the Rietveld method. The results indicate that their crystal structures are a 6H-perovskite structure with space group $P6_3/mmc$ (no. 194). The cation sites within the face-sharing octahedra of this structure are occupied by Ru ions, and those within the corner-sharing octahedra are occupied by Ln ions. Their crystal structures are the same as those of other $Ba_3LnRu_2O_9$ compounds.[13–17] The crystal structure of $Ba_3LnRu_2O_9$ is illustrated in Fig. 2 and the structural parameters are summarized in Table 1.

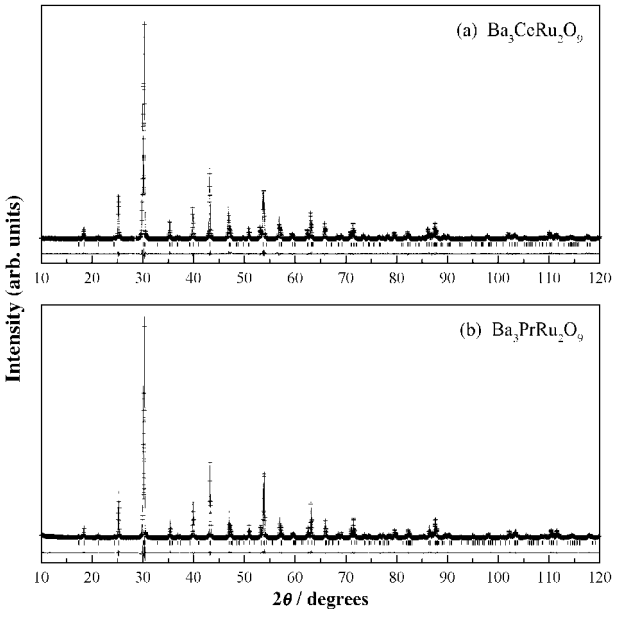

Fig. 1 X-Ray diffraction profiles for (a) $Ba_3CeRu_2O_9$ and (b) $Ba_3PrRu_2O_9$. The calculated and observed diffraction profiles are shown on the top as a solid line and cross markers, respectively. The vertical marks show positions calculated from Bragg reflections. The bottom trace is a plot of the difference between the calculated and observed intensities.

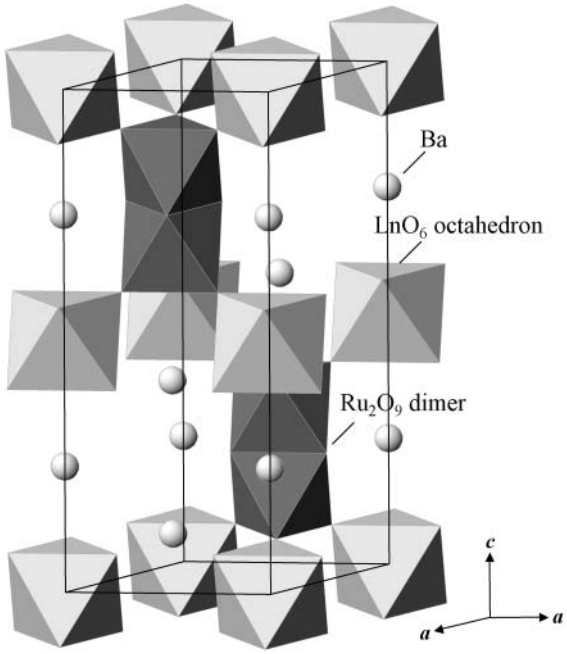

Fig. 2 The crystal structure of $Ba_3LnRu_2O_9$.

Powder neutron diffraction (ND) measurements for $Ba_3TbRu_2O_9$ were performed at 2 and 15 K, and at room temperature. Their diffraction profiles are shown in Fig. 3. The Rietveld analyses of data collected at 15 K and room temperature indicate that $Ba_3TbRu_2O_9$ adopts the 6H-perovskite structure, which is consistent with the conclusions from the XRD data. No evidence for cation disorder or oxygen defects was found. The refined structural parameters are summarized in Table 1. The data collected at 2 K show a

Table 1 Structural parameters for $Ba_3LnRu_2O_9$ (Ln = Ce, Pr, Tb)[a]

	Ce	Pr	Tb		
	XRD (RT)	XRD (RT)	ND (RT)	ND (15 K)	ND (2 K)
a/Å	5.8894(2)	5.8855(1)	5.8365(5)	5.8236(4)	5.8238(2)
c/Å	14.6476(4)	14.6071(2)	14.4257(9)	14.4096(7)	14.4088(4)
V/Å^3	439.99(3)	438.19(1)	425.56(6)	423.22(4)	423.23(2)
Ba1 B/Å^2	0.75(6)	0.51(4)	0.59(12)	0.02(8)	0.04(8)
Ba2 z	0.9025(1)	0.9036(1)	0.9066(3)	0.9063(2)	0.9063(2)
Ba2 B/Å^2	0.61(3)	0.51(2)	0.58(11)	0.11(7)	0.20(7)
Ln B/Å^2	0.19(5)	0.04(4)	0.51(9)	0.18(6)	0.33(5)
Ru z	0.1653(1)	0.1649(1)	0.1636(2)	0.1639(1)	0.1640(2)
Ru B/Å^2	0.10(3)	0.10(3)	0.48(7)	0.24(5)	0.28(4)
O1 x	0.4901(10)	0.4882(7)	0.4883(4)	0.4896(3)	0.4890(3)
O1 B/Å^2	1.2(3)	1.1(2)	0.68(7)	0.41(5)	0.49(4)
O2 x	0.1765(8)	0.1754(6)	0.1727(3)	0.1728(2)	0.1726(2)
O2 z	0.4122(4)	0.4128(4)	0.4151(1)	0.4150(1)	0.4150(1)
O2 B/Å^2	1.2(2)	0.8(1)	0.90(6)	0.46(4)	0.56(3)
R_{wp}[b] (%)	13.35	10.82	7.88	5.98	6.47
R_I[b] (%)	2.56	1.66	2.37	1.68	1.39
R_F[b] (%)	2.01	1.29	1.54	1.02	0.82
R_e[b] (%)	10.79	7.55	6.31	3.60	3.62

[a]Space group $P6_3/mmc$; $z = 2$. The atomic positions: Ba(1) 2b(0, 0, 1/4); Ba(2) 4f(1/3, 2/3, z); Ln 2a(0, 0, 0); Ru 4f(1/3, 2/3, z); O(1) 6h(x, 2x, 1/4); O(2) 12k(x, 2x, z). [b]Definitions of reliability factors R_{wp}, R_I, R_F and R_e are given as follows: $R_{wp} = [\sum w(|F_o| - |F_c|)^2 / \sum w|F_o|^2]^{1/2}$; $R_I = \sum |I_{ko} - I_{kc}| / \sum I_{ko}$; $R_F = \sum \left| I_{ko}^{\frac{1}{2}} - I_{kc}^{\frac{1}{2}} \right| / \sum I_{ko}^{\frac{1}{2}}$; $R_e = [(N-p) / \sum_i w_i y_i^2]^{1/2}$.

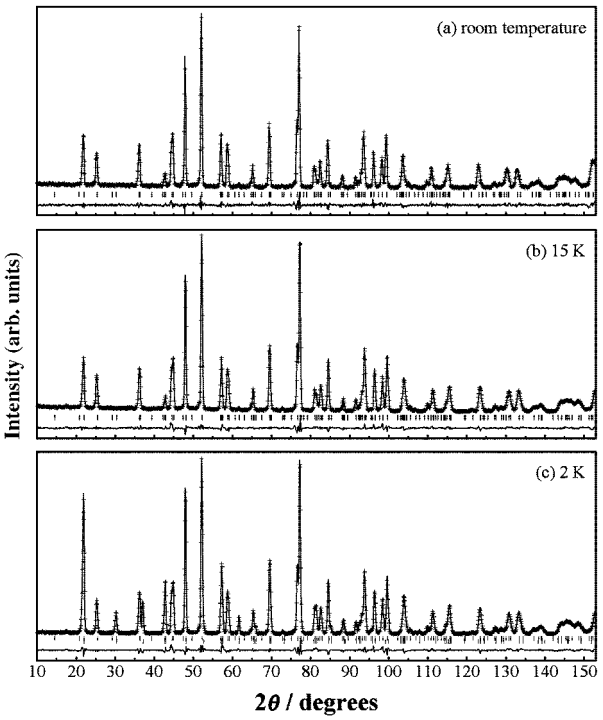

Fig. 3 Powder neutron diffraction profiles for $Ba_3TbRu_2O_9$ at room temperature (a), 15 (b) and 2 K (c). The calculated and observed diffraction profiles are shown on the top as a solid line and cross markers, respectively. The vertical marks show positions calculated from Bragg reflections. In (c), the magnetic reflection positions are shown as lower vertical marks. The bottom traces are plots of the difference between calculated and observed intensities.

number of low angle peaks, which are not observed at 15 K and room temperature. They are due to an antiferromagnetic ordering of the Tb^{4+} ions. The crystal and magnetic structures at 2 K have been determined by the Rietveld method. The crystal structure at 2 K has the same symmetry as that at 15 K and room temperature. The magnetic structure will be discussed later. A recent study of an analogous compound, $Ba_3NdRu_2O_9$, has indicated that the structural phase transition from hexagonal to monoclinic symmetry occurs at *ca.* 120 K.[16] However, $Ba_3TbRu_2O_9$ does not show any structural phase transition down to 2 K.

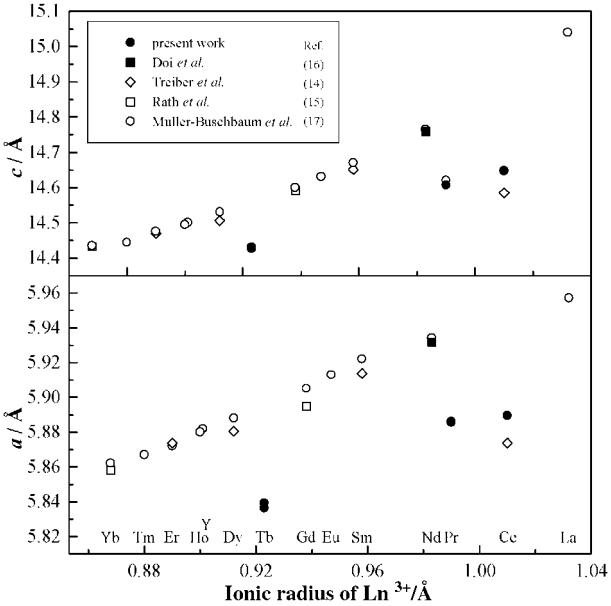

Fig. 4 Variation of lattice parameters for $Ba_3LnRu_2O_9$ with the ionic radius of Ln^{3+}.

Table 2 Selected bond lengths (Å) and angles (°) for $Ba_3LnRu_2O_9$ (Ln = Ce and Pr) at room temperature

		$Ba_3CeRu_2O_9$	$Ba_3PrRu_2O_9$
Ba(1)–O(1)	×6	2.946(5)	2.945(5)
Ba(1)–O(2)	×6	2.982(7)	2.974(5)
Ba(2)–O(1)	×3	2.869(6)	2.888(4)
Ba(2)–O(2)	×6	2.950(5)	2.947(5)
Ba(2)–O(2)	×3	3.150(7)	3.129(5)
Ru–O(1)	×3	2.024(8)	2.009(5)
Ru–O(2)	×3	1.962(8)	1.970(5)
Ru–O (average)		**1.993(8)**	**1.989(5)**
Ru–Ru		2.481(3)	2.486(2)
Ln–O(2)	×6	2.213(8)	2.195(5)
Ru–O(2)–Ln		179.9(4)	179.7(3)
Ru–O(1)–Ru		75.6(4)	76.5(3)

Table 3 Selected bond lengths (Å) and angles (°) for $Ba_3TbRu_2O_9$

		300 K	15 K	2 K
Ba(1)–O(1)	×6	2.921(2)	2.914(2)	2.914(2)
Ba(1)–O(2)	×6	2.953(3)	2.948(2)	2.946(2)
Ba(2)–O(1)	×3	2.890(4)	2.875(3)	2.878(3)
Ba(2)–O(2)	×6	2.921(2)	2.915(2)	2.915(2)
Ba(2)–O(2)	×3	3.042(4)	3.042(3)	3.043(3)
Ru–O(1)	×3	2.002(4)	2.006(3)	2.000(3)
Ru–O(2)	×3	1.982(3)	1.978(2)	1.981(2)
Ru–O (average)		**1.992(3)**	**1.992(2)**	**1.991(3)**
Ru–Ru		2.493(6)	2.482(4)	2.480(2)
Tb–O(2)	×6	2.132(3)	2.131(2)	2.129(2)
Ru–O(2)–Tb		179.9(2)	179.9(1)	179.9(1)
Ru–O(1)–Ru		77.0(2)	76.4(1)	76.6(1)

The variation of lattice parameters for $Ba_3LnRu_2O_9$ with the ionic radius of Ln^{3+} is shown in Fig. 4. The results of previous studies are also plotted in this figure. The lattice parameters for $Ba_3LnRu_2O_9$ increase monotonously with the ionic radius of Ln^{3+} from Lu to La, but those for the Ce, Pr and Tb compounds deviate substantially from this trend. We consider that the Ce, Pr and Tb ions are not in the trivalent state, but in the tetravalent state.[20] Some selected bond lengths and angles for the title compounds are listed in Tables 2 and 3. The refined Ce–O, Pr–O and Tb–O bond lengths are 2.213(8), 2.195(5) and 2.132(3) Å, respectively. These are close to the Ln^{4+}–O^{2-} lengths calculated from Shannon's ionic radii:[21] 2.27, 2.25 and 2.16 Å for Ce, Pr and Tb, respectively. These results indicate that the Ln ions in the title compounds are in the tetravalent state. This conclusion agrees with previous discussions by Müller-Buschbaum and Mertens (for the Ce compound)[17] and Treiber *et al.* (for the Pr compound).[14]

The RuO_6 octahedra in the Ru_2O_9 dimer are not regular in shape. The Ru–O(1) bond lengths [O(1) atoms are on the shared face in the Ru_2O_9 dimer] are longer than the Ru–O(2) bond lengths [O(2) atoms are on the top or bottom face of the Ru_2O_9 dimer]. The average Ru–O lengths are about 1.99 Å, which is intermediate between 1.965 Å for Ru^{5+}–O^{2-} and 2.020 Å for Ru^{4+}–O^{2-}, calculated from Shannon's ionic radii.[21] However, we consider that the ruthenium ions are most likely tetravalent in the title compounds, because the obtained lengths are very close to the Ru^{4+}–O^{2-} lengths found in other perovskites, for example, $CaRuO_3$: 1.99 Å,[22,23] $SrRuO_3$: 1.984 Å,[22,24] and $BaRuO_3$: 1.993 Å.[25]

Electrical resistivity

The temperature dependence of the resistivities of $Ba_3LnRu_2O_9$ (Ln = Ce, Pr and Tb) is plotted in Fig. 5. All the samples are nonmetallic in the temperature range studied, showing an

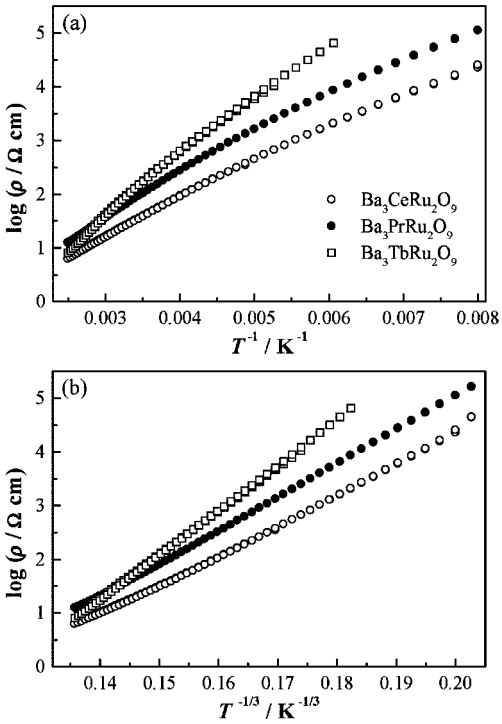

Fig. 5 Temperature dependence of the resistivity for $Ba_3LnRu_2O_9$: (a) log ρ *vs.* T^{-1} plot; (b) log ρ *vs.* $T^{-\frac{1}{3}}$ plot.

increase in resistivity with decreasing temperature. Attempts to fit the observed data to a simple Arrhenius model were unsuccessful. The Mott variable range hopping (VRH) behavior[26]

$$\rho \propto \exp[(T_0/T)^v] \tag{1}$$

was taken into account. When the parameter v is $\frac{1}{3}$, the experimental data show good linearity [Fig. 5(b)]. The resistivity of the isostructural compounds $Ba_3MRu_2O_9$ (M = Fe, Co, Ni, Cu and In) was reported previously, and it was found that the plots of log ρ *vs.* $T^{-\frac{1}{3}}$ are linear.[27] Our results also suggest that the semiconducting behavior of $Ba_3LnRu_2O_9$ may be attributed to variable range hopping in two dimensions.[26]

Magnetic susceptibilities

The temperature dependence of the ZFC and FC magnetic susceptibilities for $Ba_3PrRu_2O_9$ is plotted in Fig. 6. They increase gradually above 100 K. In addition, they show an anomaly at 10.5 K and divergence between the ZFC and FC susceptibilities is observed below this temperature. Both the Ru^{4+} ions ($4d^4$) and Pr^{4+} ions ($4f^1$) should contribute to the magnetic susceptibility of $Ba_3PrRu_2O_9$. The Ru^{4+} ions form Ru_2O_9 dimers in this compound. The magnetic behavior above 100 K resembles that found in $Ba_3M^{2+}Ru^{5+}{}_2O_9$ (M^{2+} is nonmagnetic) reported by Darriet *et al.*[9] They explained the magnetic behavior using a simple model: the Hamiltonian for the magnetic interaction of Ru ions in the Ru_2O_9 dimers is written as

$$\boldsymbol{H} = -2J\boldsymbol{S}_1\cdot\boldsymbol{S}_2 \tag{2}$$

where $\boldsymbol{S}_1$ and $\boldsymbol{S}_2$ are the spin operators and J is the exchange integral in the dimer.

We have attempted to apply this model to the present results. The temperature dependence of the magnetic susceptibility for $Ru^{4+}{}_2O_9$ dimers should be represented by

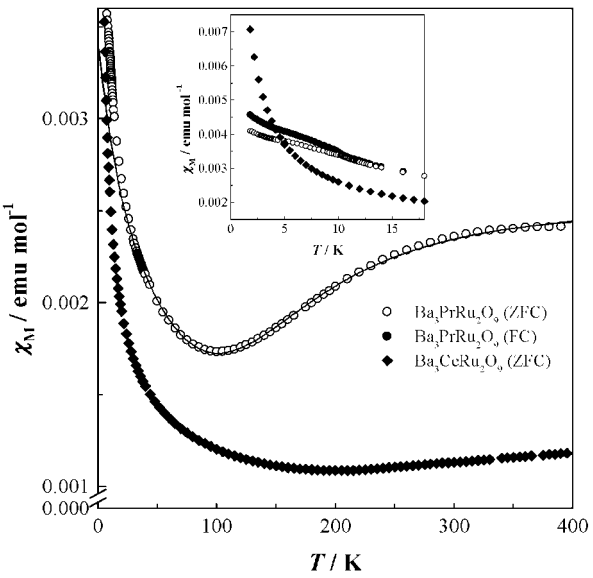

Fig. 6 Temperature dependence of the magnetic susceptibilities of $Ba_3CeRu_2O_9$ and $Ba_3PrRu_2O_9$. The applied field is 0.1 T. The inset shows the magnetic susceptibilities at low temperatures. The solid lines are the susceptibilities calculated from eqn. (6) for the low spin and the high spin models. In this figure, they overlap.

$$\chi_{\text{dimer}} = \frac{N_A g^2 \mu_B^2}{3k_B T} \times \frac{6(x^4+5)}{x^6+3x^4+5} \tag{3}$$

or

$$\chi_{\text{dimer}} = \frac{N_A g^2 \mu_B^2}{3k_B T} \times \frac{6(x^{18}+5x^{14}+14x^8+30)}{x^{20}+3x^{18}+5x^{14}+7x^8+9} \tag{4}$$

where $x = \exp(J/k_BT)$, and N_A, g, μ_B and k_B are the Avogadro number, g factor, Bohr magneton and Boltzmann constant, respectively. Eqn. (3) and (4) express the magnetic susceptibility for the low spin ($S_1 = S_2 = 1$) and high spin ($S_1 = S_2 = 2$) dimers, respectively. The observed susceptibilities of $Ba_3PrRu_2O_9$ show Curie–Weiss-like behavior at low temperatures. The Curie–Weiss term

$$\chi_{\text{CW}} = \frac{C}{T-\theta} \tag{5}$$

is added to the expression for the dimers, χ_{dimer} [eqn. (3) and (4)]

$$\chi = \chi_{\text{dimer}} + \chi_{\text{CW}} + \chi_{\text{TIP}} \tag{6}$$

where C, Θ and χ_{TIP} are the Curie constant, the Weiss temperature and the temperature independent paramagnetic susceptibility, respectively. In order to explain the temperature dependency of the magnetic susceptibility, eqn. (6) was fitted to the experimental data above 30 K. The solid lines in Fig. 6 represent the fitting results, and the following parameter values are determined from these fits: $g = 1.98(2)$, $J/k_B = -281(1)$ K, $C = 0.096(8)$ emu K mol^{-1}, $\Theta = -38(4)$ K and $9.2(4) \times 10^{-4}$ emu mol^{-1} (for the low spin model) or $g = 1.98(2)$, $J/k_B = -280(1)$ K, $C = 0.10(1)$ emu K mol^{-1}, $\Theta = -40(4)$ K and $9.0(4) \times 10^{-4}$ emu mol^{-1} (for the high spin model). Both calculated susceptibilities are in comparatively good agreement with the experimental data. There is not a large difference between the two calculated curves in this temperature range; accordingly, it cannot be determined whether the high spin or low spin state is adopted.

The Curie–Weiss term of eqn. (6) would be due to the paramagnetism of the Pr^{4+} ions. The effective magnetic moment is about 0.9 μ_B, which is much smaller than that expected for a free f^1 ion (2.54 μ_B). This indicates that the

crystal field with octahedral symmetry has a significant effect on the magnetic properties of Pr^{4+}. A comparably small magnetic moment has been reported for the perovskites $Ba_{1-x}Sr_xPrO_3$.[28] The value of J is *ca.* −280 K, which indicates the presence of an antiferromagnetic interaction in the dimers. The magnitude of this J value is larger than in most of the $Ru^{5+}{}_2O_9$ dimers ($S_1 = S_2 = \frac{3}{2}$; $J \approx -170$ K).[9,10] This means that the magnetic interaction in the $Ru^{4+}{}_2O_9$ dimers is stronger than that in the $Ru^{5+}{}_2O_9$ dimers. The difference in the Ru–Ru distance may be one of the causes for this phenomenon. The Ru–Ru distance in the $Ru^{4+}{}_2O_9$ dimers is ~2.48 Å, which is much shorter than that in the $Ru^{5+}{}_2O_9$ dimers (2.65–2.76 Å).[9,12,29,30]

The temperature dependence of the ZFC magnetic susceptibility for $Ba_3CeRu_2O_9$ is also shown in Fig. 6. No divergency between the ZFC and FC susceptibilities has been found throughout the experimental temperature range. At low temperature, no magnetic anomalies have been observed, that is the susceptibilities of $Ba_3CeRu_2O_9$ decrease with increasing temperature. However, they increase slightly with temperature above 200 K. Only the $Ru^{4+}{}_2O_9$ ($4d^4$) dimers should contribute to the magnetic susceptibility of this compound, because the other ions are nonmagnetic. We tried to fit the observed susceptibility data using the same dimer model [eqn. (6)]. However, a good agreement between the observed and calculated susceptibilities was not obtained. Therefore, the magnetic properties of $Ba_3CeRu_2O_9$ do not obey the simple dimer model. In order to explain this magnetic behavior, further magnetic measurements in the higher temperature range are needed.

The temperature dependence of the magnetic susceptibility of $Ba_3TbRu_2O_9$ is plotted in Fig. 7. The susceptibility shows a maximum at 9.5 K and decreases rapidly with decreasing temperature below this point, indicating the occurrence of an antiferromagnetic transition. Below the transition temperature, the ZFC and FC susceptibilities diverge. Attempts to fit the observed susceptibility using the same dimer model [eqn. (6)] were unsuccessful. One reason for this may come from the fact that the magnetic susceptibility of the paramagnetic Tb^{4+} ions should be much larger than that of the dimers. The higher temperature data ($T > 100$ K) can be fitted using the Curie–Weiss law. The obtained effective magnetic moment and Weiss constant are 7.93(1) μ_B and −2.8(3) K, respectively. This effective magnetic moment is close to that for Tb^{4+} ions

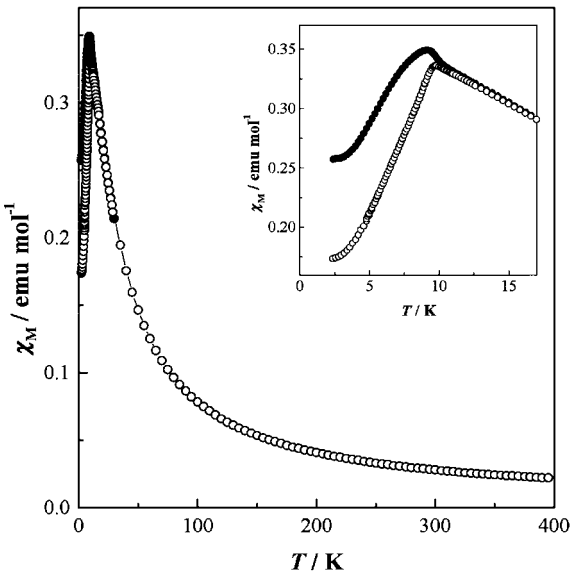

Fig. 7 Temperature dependence of the magnetic susceptibilities of $Ba_3TbRu_2O_9$. The open and filled symbols show the ZFC and FC susceptibilities, respectively. The applied field is 0.1 T.

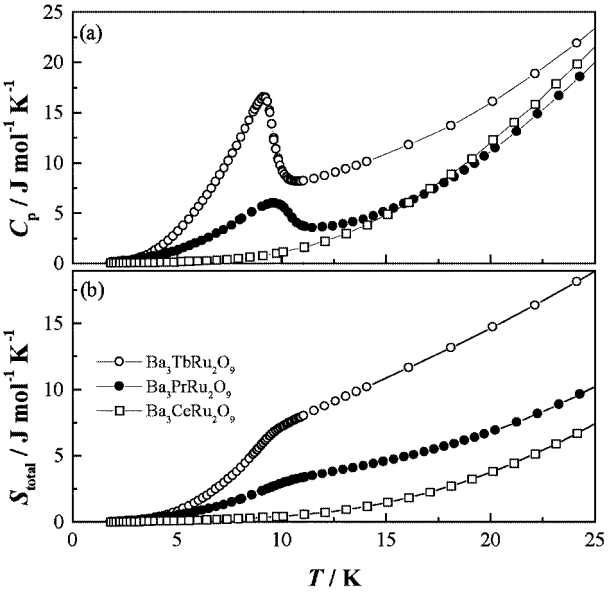

Fig. 8 Temperature dependences of the specific heat (a) and the total entropy (b) for $Ba_3LnRu_2O_9$.

(7.94 μ_B) rather than that for Tb^{3+} ions (9.72 μ_B). The field dependence of the magnetization was measured at 5 and 20 K. A small hysteresis loop was observed at 5 K, and it has a remnant magnetization of ~0.01 μ_B. This small ferromagnetic moment may be attributed to a weak ferromagnetism associated with the antiferromagnetism.[31]

Specific heat

Fig. 8(a) shows the variation of the specific heat for $Ba_3LnRu_2O_9$ (Ln = Ce, Pr and Tb) as a function of temperature. The specific heat measurements for $Ba_3PrRu_2O_9$ and $Ba_3TbRu_2O_9$ show λ-type anomalies at 10.5 and 9.5 K, respectively, which correspond to the magnetic anomalies found in the magnetic susceptibilities. These facts indicate that an Ln^{4+} antiferromagnetic transition occurs at these temperatures. The temperature dependence of the total entropy has been calculated from the specific heat data, and is shown in Fig. 8(b). If it is assumed that the electronic and lattice contributions to the specific heat are equal among these three compounds, the difference in the total entropy between the Ce and Pr compounds (or between the Ce and Tb compounds) should be equal to the magnetic entropy of Pr^{4+} (or Tb^{4+}). The magnetic entropies of Pr^{4+} and Tb^{4+} estimated at 15 K are 3.2 and 9.5 J mol^{-1} K^{-1}, respectively. The ground state $^2F_{5/2}$ of the Pr^{4+} ion is split into a doublet (Γ_7) and a quartet (Γ_8) in the octahedral symmetry. The magnetic entropy change of $Ba_3PrRu_2O_9$ is close to $R\ln 2 = 5.76$ J mol^{-1} K^{-1} rather than $R\ln 4 = 11.53$ J mol^{-1} K^{-1}, which suggests that the ground state is Γ_7. The effective magnetic moment obtained from the experimental data (*ca.* 0.9 μ_B) is close to that expected from this ground state: $g_J\sqrt{J_z(J_z+1)} = \frac{6}{7}\sqrt{\frac{5}{6}\left(\frac{5}{6}+1\right)} = 1.06\ \mu_B$. The magnetic entropy change of $Ba_3TbRu_2O_9$ is 9.5 J mol^{-1} K^{-1}, which is smaller than that expected from $R\ln(2S+1) = R\ln 8 = 17.29$ J K^{-1} mol^{-1}. The cause for this discrepancy is not clear at present. There may be a short range magnetic ordering of Tb^{4+} ions above the magnetic transition temperature.

Magnetic structure of $Ba_3TbRu_2O_9$

As has been mentioned earlier, some magnetic reflection peaks were observed in the neutron diffraction data collected at 2 K (see Fig. 3). All magnetic peaks are indexed in the crystallographic unit cell with odd values of l; however, the (001) peak (2θ = *ca.* 7.2°) and other (00l) peaks are negligibly weak. These facts indicate that two Tb^{4+} ions occupying the 2*a* Wyckoff

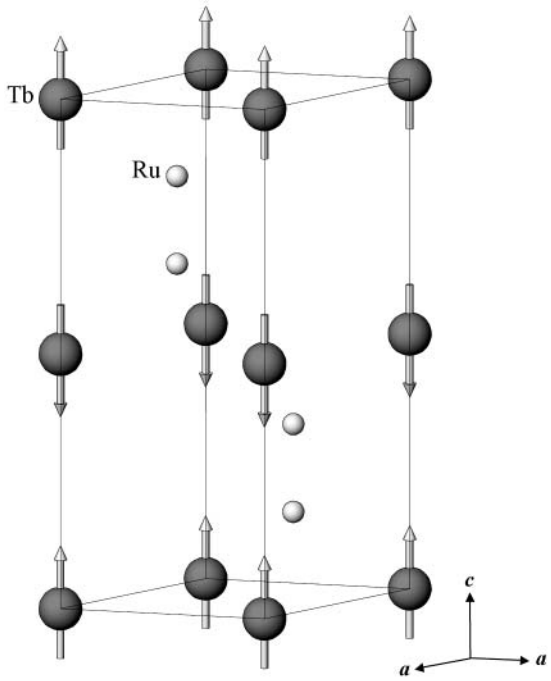

Fig. 9 The magnetic structure of $Ba_3TbRu_2O_9$ at 2 K. Diamagnetic ions are omitted. The arrows indicate the directions of the magnetic moments. The ordered magnetic moment of Tb^{4+} is 6.84(4) μ_B; the direction of the magnetic moments is [001].

positions have antiparallel magnetic moments with each other, and that the direction of ordered moments is parallel to the *c* axis. On the other hand, the ordered moments of Ru ions were not determined. This may be due to an absence of long range magnetic ordering of the Ru_2O_9 dimers. The magnetic structure of $Ba_3TbRu_2O_9$ is illustrated in Fig. 9. In this magnetic structure, the magnetic moments of the Tb^{4+} ions order ferromagnetically in the *c* plane, and these ferromagnetic sheets are stacked antiferromagnetically along the *c* axis. The direction of ordered moments is parallel to the *c* axis. The ordered magnetic moment of Tb^{4+} ions is 6.84(4) μ_B. This value is reasonable for Tb^{4+} ($4f^7$) and comparable to those of other perovskites containing Tb^{4+} ions: 6.76 ($SrTbO_3$) and 6.5 μ_B ($BaTbO_3$) at 10 K.[31]

Conclusion

Rietveld analyses of the X-ray and neutron diffraction data for the 6H-perovskites $Ba_3LnRu_2O_9$ (Ln = Ce, Pr and Tb) were performed. The Ru ions occupy the face-sharing octahedral sites, while the Ln ions occupy the corner-sharing octahedral sites. The oxidation states of both Ru and Ln ions are tetravalent. These compounds are semiconductors over the temperature range 100–400 K. The magnetic susceptibilities and specific heat for $Ba_3LnRu_2O_9$ were measured. It was found that an Ln^{4+} antiferromagnetic transition occurred at 9.5 (Ln = Tb) and 10.5 K (Ln = Pr) and that $Ba_3PrRu_2O_9$ showed magnetic behavior due to the $Ru^{4+}{}_2O_9$ dimer in the higher temperature range. The magnetic susceptibility of $Ba_3CeRu_2O_9$ increases with temperature above 200 K. However, this behavior cannot be explained by the dimer model. Powder neutron diffraction measurements for $Ba_3TbRu_2O_9$ at 2 K show that long range antiferromagnetic ordering of Tb^{4+} ions exists, and the magnetic structure was determined by the Rietveld analysis.

In order to clarify the magnetic behavior of $Ba_3CeRu_2O_9$ and to determine the exact *J* value of the $Ru^{4+}{}_2O_9$ dimer, further magnetic measurements at higher temperatures are needed.

Acknowledgements

This work was supported by The Iwatani Naoji Foundation's Research Grant. One of us (Y. D.) is grateful for a Research Fellowship for Young Scientists from the Japan Society for the Promotion of Science.

References

1 A. Callaghan, C. W. Moeller and R. Ward, *Inorg. Chem.*, 1966, **5**, 1572.
2 Y. Maeno, H. Hashimoto, K. Yoshida, S. Nishizaki, T. Fujita, J. G. Bednorz and F. Lichtenberg, *Nature (London)*, 1994, **372**, 532.
3 P. D. Battle and C. W. Jones, *J. Solid State Chem.*, 1991, **90**, 302.
4 Y. Doi and Y. Hinatsu, *J. Phys.: Condens. Matter*, 1999, **11**, 4813.
5 Y. Doi, Y. Hinatsu, K. Oikawa, Y. Shimojo and Y. Morii, *J. Mater. Chem.*, 2000, **10**, 797.
6 Y. Izumiyama, Y. Doi, M. Wakeshima, Y. Hinatsu, K. Oikawa, Y. Shimojo and Y. Morii, *J. Mater. Chem.*, 2000, **10**, 2364.
7 Y. Izumiyama, Y. Doi, M. Wakeshima, Y. Hinatsu, Y. Shimojo and Y. Morii, *J. Phys.: Condens. Matter*, 2001, **13**, 1303.
8 R. D. Burbank and H. T. Evans, *Acta Crystallogr.*, 1948, **1**, 330.
9 J. Darriet, M. Drillon, G. Villeneuve and P. Hagenmuller, *J. Solid State Chem.*, 1976, **19**, 213.
10 J. Darriet, J. L. Soubeyroux and A. P. Murani, *J. Phys. Chem. Solids*, 1983, **44**, 269.
11 R. C. Byrne and C. W. Moeller, *J. Solid State Chem.*, 1970, **2**, 228.
12 P. Lightfoot and P. D. Battle, *J. Solid State Chem.*, 1990, **89**, 174.
13 I. Thumm, U. Treiber and S. Kemmler-Sack, *Z. Anorg. Allg. Chem.*, 1981, **477**, 161.
14 U. Treiber, S. Kemmler-Sack, A. Ehmann, H.-U. Schaller, E. Dürrschmidt, I. Thumm and H. Bader, *Z. Anorg. Allg. Chem.*, 1981, **481**, 143.
15 M. Rath and H. Müller-Buschbaum, *J. Alloys Compd.*, 1994, **210**, 119.
16 Y. Doi and Y. Hinatsu, *J. Solid State Chem.*, 2001, **161**, in press.
17 H. Müller-Buschbaum and B. Mertens, *Z. Naturforsch., B: Chem.*, 1996, **51**, 79.
18 K. Ohoyama, T. Kanouchi, K. Nemoto, M. Ohashi, T. Kajitani and Y. Yamaguchi, *Jpn. J. Appl. Phys.*, 1998, **37**, 3319.
19 F. Izumi and T. Ikeda, *Mater. Sci. Forum*, 2000, **321–324**, 198.
20 D. Harada, M. Wakeshima and Y. Hinatsu, *J. Solid State Chem.*, 1999, **145**, 356.
21 R. D. Shannon, *Acta Crystallogr., Sect. A*, 1976, **32**, 751.
22 H. Kobayashi, M. Nagata, R. Kanno and Y. Kawamoto, *Mater. Res. Bull.*, 1994, **29**, 1271.
23 W. Bensch, H. W. Schmalle and A. Reller, *Solid State Ionics*, 1990, **43**, 171.
24 C. W. Jones, P. D. Battle and P. Lightfoot, *Acta Crystallogr., Sect. C*, 1989, **45**, 365.
25 P. C. Donohue, L. Katz and R. Ward, *Inorg. Chem.*, 1965, **4**, 306.
26 N. F. Mott and E. A. Davis, *Electronic Processes in Non-Crystalline Materials*, Clarendon Press, Oxford, UK, 2nd edn., 1979.
27 J. T. Rijssenbeek, P. Matl, B. Batlogg, N. P. Ong and R. J. Cava, *Phys. Rev. B: Condens. Matter*, 1998, **58**, 10315.
28 Y. Hinatsu, *J. Solid State Chem.*, 1995, **119**, 405.
29 H. W. Zandbergen and D. J. Ijdo, *Acta Crystallogr., Sect. C*, 1984, **40**, 919.
30 J. Wilkens and H. Müller-Buschbaum, *Z. Anorg. Allg. Chem.*, 1993, **619**, 517.
31 K. Tezuka, Y. Hinatsu, Y. Shimojo and Y. Morii, *J. Phys.: Condens. Matter*, 1998, **10**, 11703.